Effective Constitutive Parameters of High-Temperature Superconducting Split-Ring Resonator Arrays

Frank Trang, Horst Rogalla, *Senior Member, IEEE*, and Zoya Popović, *Fellow, IEEE*

***Abstract*—The effective constitutive parameters of a high-temperature superconducting (HTS) metamaterial are extracted from measured scattering parameters at liquid nitrogen temperature (≈75.68 K at the National Institute of Standards and Technology, Boulder, CO, USA). The $YBa_2Cu_3O_7$ split-ring resonator (SRR) arrays are placed inside a WR-90 waveguide with two different orientations and are excited with the dominant TE_{10} mode in both cases. By treating the SRR array as a homogeneous medium described by the biaxial permittivity and permeability diagonal tensors, the two sets of S parameters allow for the extraction of three out of the six tensor components. The extracted parameters are then compared to full-wave simulations of SRR arrays in free space. The samples are measured from 8.2 to 12 GHz and show a frequency band between 9.25 and 10.45 GHz with a negative effective permeability, as expected. Finally, numerous high-quality factor resonances that accompany the main resonances are observed in both the low-temperature measurement and the low-loss simulation.**

***Index Terms*—High-temperature superconducting (HTS), magnesium oxide (MgO), split-ring resonators (SRRs), yttrium barium copper oxide (YBCO).**

I. Introduction

THERE have been many proposed methods for characterizing the effective constitutive parameters of split-ring resonator (SRR) arrays, with a purpose of demonstrating the existence of an effective negative permeability over some frequency band. For example, in [1]–[5], the plane wave normal incidence approach was discussed for retrieving the effective parameters; in [6], an optimization technique was presented; and in [7], a waveguide approach for retrieving the anisotropic parameters was presented. Applications that take advantage of the effective near-zero and negative permeability property of SRRs include negative index materials [8], [9] and electromagnetic cloaks [10], [11]. The circuits in these studies use normal metal and exhibit loss that limits their performance and can be reduced by using superconductors. In this paper, we present the extracted effective relative permittivity and permeability of high-temperature superconducting (HTS) SRR arrays. Of the listed method, we find that the waveguide method in [7] is best suited to our experimental study of the effective permittivity and permeability tensors of HTS SRR arrays since the waveguide setup is confined to a small space, which can be cooled easily as demonstrated by Trang *et al.* [12]. Another waveguide retrieval method theoretically proposed by Damaskos *et al.* [13] requires measurements of the samples with the waveguide excited by both the TE_{10} and the TE_{20} modes, which would be difficult to accomplish experimentally. Other studies on superconducting metamaterials have been presented by Ricci *et al.* [14]–[16] and Chen *et al.* [17], but the quantitative effective constitutive parameters were not discussed. In [12], the relative effective permittivity and permeability of HTS yttrium barium copper oxide (YBCO) SRRs are extracted by assuming homogeneous and isotropic bulk properties.

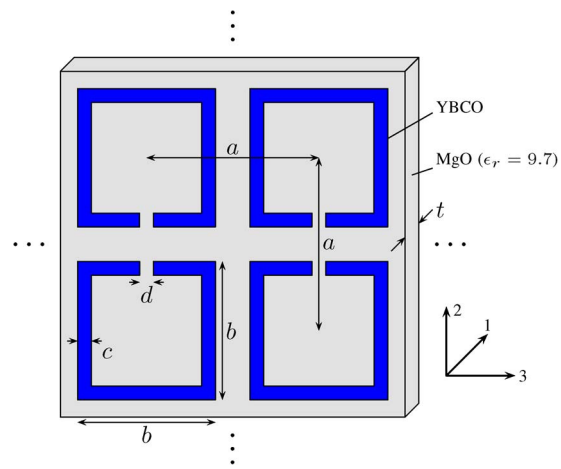

Fig. 1. Sketch of an experimental X-band YBCO SRR array deposited on a MgO substrate with $a = 2.5$ mm, $b = 2$ mm, $c = 0.2$ mm, $d = 0.2$ mm, and $t = 0.5$ mm. The material axes 1, 2, and 3 correspond with the tensor elements $\bar{\bar{\epsilon}}$ and $\bar{\bar{\mu}}$.

In this paper, we present the extracted effective relative permittivity and permeability of YBCO SRR arrays deposited on a magnesium oxide (MgO) substrate, as shown in Fig. 1. The arrays are measured inside a WR-90 X-band waveguide at liquid nitrogen (LN_2) temperature. YBCO has a critical temperature of ≈88 K [18], above the boiling temperature of LN_2 (≈75.68 K at 1655 m elevation in Boulder, CO, USA). The free-space wavelength at 10 GHz is greater than ten times the SRR array spatial period, and thus, the array can be thought of as having effective parameters. We will show that in the frequency band where the real part of the relative permeability

Manuscript received December 18, 2013; revised April 16, 2014; accepted July 27, 2014. Date of publication August 19, 2014; date of current version November 26, 2014. This work was supported by the U.S. Air Force (AFOSR) through Grant FA9550-10-1-0413. This paper was recommended by Associate Editor D. E. Oates.

The authors are with the Department of Electrical, Computer, and Energy Engineering, University of Colorado, Boulder, CO 80309 USA (e-mail: frank.trang@colorado.edu).

Color versions of one or more of the figures in this paper are available online at http://ieeexplore.ieee.org.

Digital Object Identifier 10.1109/TASC.2014.2349507

1051-8223 © 2014 IEEE. Personal use is permitted, but republication/redistribution requires IEEE permission.
See http://www.ieee.org/publications_standards/publications/rights/index.html for more information.

μ' is negative, the imaginary part μ'' quickly drops to near zero. The effective parameters extracted from the scattering (S) parameters treat the SRR array as a homogeneous medium described by the biaxial relative permittivity and permeability tensors $\bar{\bar{\epsilon}} = \mathrm{diag}[\epsilon_1, \epsilon_2, \epsilon_3]$ and $\bar{\bar{\mu}} = \mathrm{diag}[\mu_1, \mu_2, \mu_3]$, respectively. The time convention followed in this paper is $e^{j\omega t}$ with $\epsilon = \epsilon' - j\epsilon''$ and $\mu = \mu' - j\mu''$.

The SRR specifications and measurement setup will first be discussed, followed by an outline of the extraction method used to calculate the tensor elements from the measured and simulated S parameters. Arrays of the SRRs are placed inside the waveguide with two orthogonal orientations and the respective scattering parameters recorded. Measurements from the two orientations discussed in this paper allow for the retrieval of three of the six tensor elements, i.e., μ_1, ϵ_2, and μ_3, with the material indices shown in Fig. 1. The other three elements can be retrieved in a similar manner by measuring the samples with two different orientations, as discussed in [7], but they are not needed for our experiments and were therefore not calculated. The retrieved parameters are then compared with those from the waveguide and free-space full-wave simulations of identical SRR arrays. Finally, we briefly discuss the additional high Q-factor resonances, accompanying the main resonances, that are only seen in the cryogenic measurement and simulations of low-loss samples.

II. SRR Specifications and Measurement Setup

Each SRR is made of a 700-nm-thick YBCO split-ring deposited on a 500-μm-thick MgO substrate, which has a nominal relative permittivity of 9.7 and at 77 K an electric loss tangent of 5×10^{-6} at 10.48 GHz [19]. The relevant dimensions are shown in Fig. 1. A single contact mask was used for patterning the SRR arrays on a 50.8×50.8 mm^2 YBCO/MgO square wafer. After etching, a 200-μm resinoid blade was used to dice 4×1 and 4×9 samples, of dimensions 10×2.5 mm^2 and 10×22.5 mm^2, respectively. The diced 4×1 and 4×9 samples have dimensions of 9.95×2.35 and 22.35×10 mm^2, respectively. This slight deviation in dimensions has a negligible effect on our results. The SRR dimensions are chosen such that the magnetic plasma frequency, which is defined as the frequency where the real part of the effective permeability is equal to zero, falls in the X-band region. The center-frequency free-space wavelength $\lambda_0 = 3$ cm is greater than ten times the SRR array spatial period a; thus, $a \ll \lambda_0$ is a valid approximation [4]. In this limit, we can treat the structure as having effective material parameters.

A waveguide thru-reflect-line calibration was performed on an Agilent 8722ES vector network analyzer (VNA) at liquid nitrogen temperature ($\approx$76 K) to set the calibrated reference planes (CRPs) to the end of the waveguide adapters. By performing the calibration at low temperature, we take into account the enhanced electrical conductivity of the metallic waveguide structures. For measurement of each calibration standard, the whole structure (waveguide adapters and standard) is wrapped with aluminum foil to prevent LN_2 seeping into the waveguide components and altering the measured phase because LN_2 has a higher dielectric constant (1.538 [20]) than air. The same cooling method was used for measuring the samples. Finally, we note that the CRPs and the material reference planes are different, as shown in Fig. 2. Thus, the measured S parameters had to be further deembedded by postprocessing the measured calibrated data.

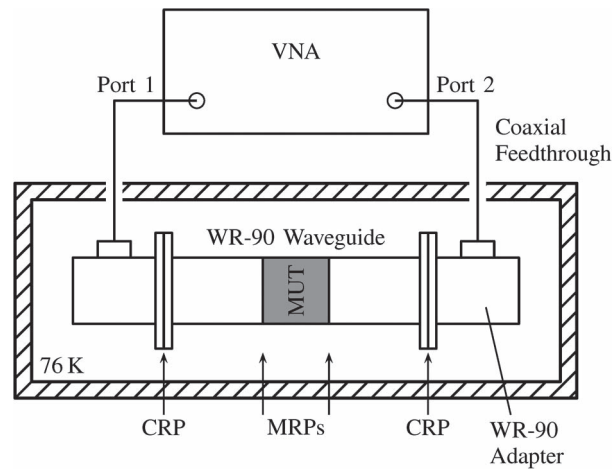

Fig. 2. Measurement setup showing the CRPs and the material under test (MUT) reference planes (MRPs). The portion inside the hashed box is cooled to $\approx$76 K. The arrows indicate the locations for the calibration and material reference planes.

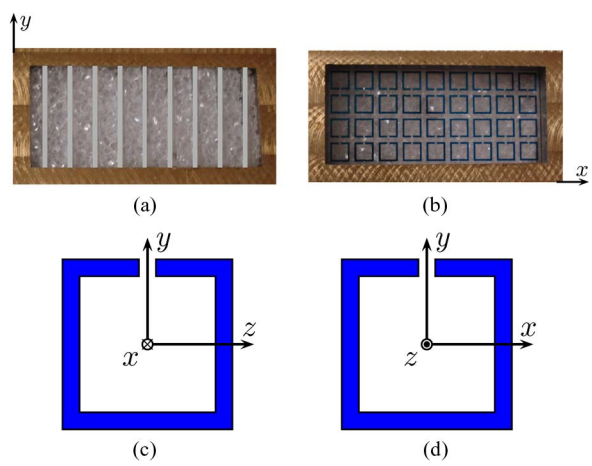

Fig. 3. Photographs of diced 4×1 and 4×9 YBCO SRR arrays on MgO substrates aligned inside a WR-90 waveguide with orientations (a) I and (b) II, respectively. The gray bars in (a) mark the locations of the 4×1 strips. The material axes corresponding to the Cartesian axes are shown for orientations (c) I and (d) II.

III. Extraction Method

Arrays of the HTS SRRs are placed inside an X-band rectangular waveguide, with orientations I and II shown in Fig. 3(a) and (b), respectively. For orientation I, nine evenly spaced 4×1 SRR strips were axially inserted into the waveguide, totaling 36 SRRs. For the rest of this paper, this will be referred to as the 4×1 strip array. A single 4×9 sample was used for the transverse orientation II, again with 36 SRRs. Note that alternating rows of the conducting SRRs in Fig. 3(a) and (b) are flipped. This is done so that when the image theory is applied along the waveguide walls, the arrays look infinitely periodic in the x and y directions. In addition, as pointed out by

Smith *et al.* [21], the symmetrical arrangement of the SRRs, as in our case, reduces the magnetoelectric coupling that is responsible for the bianisotropic behavior. For both cases, the dominant TE_{10} mode is excited in the waveguide, which has the electric field in the y direction [see Fig. 3(c) and (d)], or along material axis 2.

In order for these resonating elements to have effective properties, an effective length L has to be defined. Thus, the propagation factor through this effective material is given by

$$P = e^{-jk_{0z}nL} \tag{1}$$

where n is the effective refractive index, and k_{0z} is the longitudinal wavenumber of an empty waveguide. The anisotropic nature of the SRRs implies that we should expect two different effective indices, i.e., n_{I} and n_{II}, when measuring the sample along two different axes. An analogous way of studying n_{I} and n_{II} is to measure them along a single axis, but with the SRR structure rotated, as with orientations I and II.

The period of the SRR array is 2.5 mm. Thus, 2.5 mm was chosen for L in orientation II. The 4×1 sample width is 2.35 mm. This slight deviation from the designed value of 2.5 mm was a result of dicing imperfection. We thus used $L = 2.35$ mm for orientation I. If this L is changed to 2.5 mm instead, the value for $\min[\mathrm{Re}(\mu_1)]$ is equal to -6.8 rather than -7.3, as shown in Fig. 5(a). However, the frequency of $\min[\mathrm{Re}(\mu_1)]$ is not affected, neither is the magnetic resonant frequency. As derived by Nicolson and Ross [22] and Weir [23], the scattering parameters are related to the refractive index and normalized wave impedance ζ normalized to $\zeta_0 = \omega\mu_0/k_{0z}$ by

$$\Gamma = \frac{S_{11}^2 + 1 - S_{21}^2}{2S_{11}} \pm \sqrt{\left(\frac{S_{11}^2 + 1 - S_{21}^2}{2S_{11}}\right)^2 - 1} \tag{2}$$

$$P \equiv e^{-jk_{0z}nL} = \frac{S_{21} + S_{11} - \Gamma}{1 - (S_{21} + S_{11})\Gamma} \tag{3}$$

$$\zeta = \frac{1+\Gamma}{1-\Gamma} \tag{4}$$

$$n = \frac{1}{k_{0z}L}\left(\mathrm{Im}\left[\ln\frac{1}{P}\right] + 2\pi m\right) - \frac{j}{k_{0z}L}\mathrm{Re}\left[\ln\frac{1}{P}\right]. \tag{5}$$

Note that Γ is the reflection coefficient at the air-sample boundary if the sample extends semi-infinitely in the propagation direction. The sign in (2) is chosen such that $|\Gamma| \leq 1$. The real part of n has an ambiguity of $2\pi m$, where m is chosen so that n is a continuous function. By measuring the scattering parameters with the two orientations shown in Fig. 3, we can retrieve μ_1, ϵ_2, and μ_3. These parameters are related to the refractive index and normalized wave impedance by

$$n_{\mathrm{I}} = \frac{\sqrt{k_0^2\mu_1\epsilon_2 - k_x^2\frac{\mu_1}{\mu_3}}}{\sqrt{k_0^2 - k_x^2}} \qquad \zeta_{\mathrm{I}} = \frac{\mu_1\sqrt{k_0^2 - k_x^2}}{\sqrt{k_0^2\mu_1\epsilon_2 - k_x^2\frac{\mu_1}{\mu_3}}} \tag{6}$$

$$n_{\mathrm{II}} = \frac{\sqrt{k_0^2\mu_3\epsilon_2 - k_x^2\frac{\mu_3}{\mu_1}}}{\sqrt{k_0^2 - k_x^2}} \qquad \zeta_{\mathrm{II}} = \frac{\mu_3\sqrt{k_0^2 - k_x^2}}{\sqrt{k_0^2\mu_3\epsilon_2 - k_x^2\frac{\mu_3}{\mu_1}}} \tag{7}$$

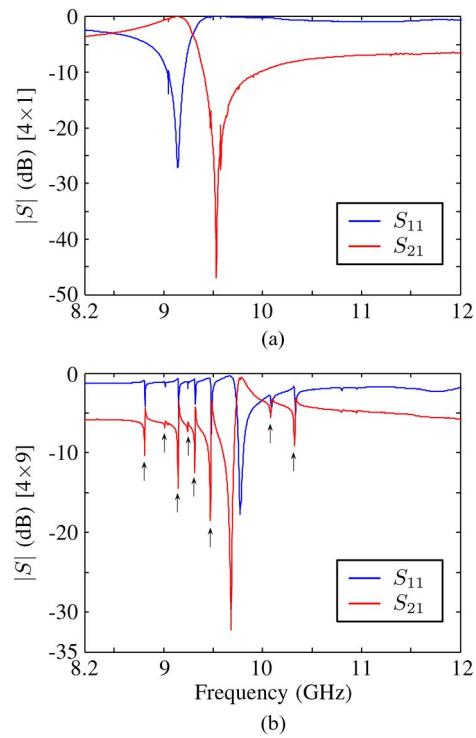

Fig. 4. Measured reflection (S_{11}, blue curve) and transmission (S_{21}, red curve) coefficient magnitudes of the (a) nine 4×1 SRR strips and (b) 4×9 SRR array, respectively, placed inside the waveguide section with the whole structure cooled to ≈76 K. The markers in (b) indicate the locations of the sharp Fano-like resonances.

resulting in formulas for the constitutive parameters

$$\mu_1 = n_{\mathrm{I}}\zeta_{\mathrm{I}} \tag{8}$$

$$\mu_3 = n_{\mathrm{II}}\zeta_{\mathrm{II}} \tag{9}$$

$$\epsilon_{2(\mathrm{I})} = \frac{n_{\mathrm{I}}^2 k_{0z}^2 + k_x^2\frac{\mu_1}{\mu_3}}{k_0^2\mu_1} \tag{10}$$

$$\epsilon_{2(\mathrm{II})} = \frac{n_{\mathrm{II}}^2 k_{0z}^2 + k_x^2\frac{\mu_3}{\mu_1}}{k_0^2\mu_3} \tag{11}$$

where $k_0 = \omega\sqrt{\mu_0\epsilon_0}$, and k_x is the waveguide cutoff wavenumber of the dominant TE_{10} mode.

IV. Experimental Results

Using a ProtoMat S62 PCB milling machine, deep grooves were milled on a Rohacell 51 IG foam to be used as sample holders for the 4×1 SRR strips. The sample holders ensure equal separation between the samples and prevent them from moving during the measurements. The Rohacell foam has a room temperature relative permittivity of 1.07 and a loss tangent of 0.0021 at 10 GHz [24], which is very similar to the electromagnetic properties of air. Properties of the foam at 77 K are not available. The SRR samples with the foam (orientation I) and without the foam (orientation II) are then placed inside a WR-90 waveguide for measurement, as shown in Fig. 3(a) and (b), respectively.

For each of the two measurements, the S parameters were deembedded to the material reference planes, with the transmission and reflection coefficients shown in Fig. 4. The stopband about 9.5 GHz in Fig. 4(a) suggests a region of negative

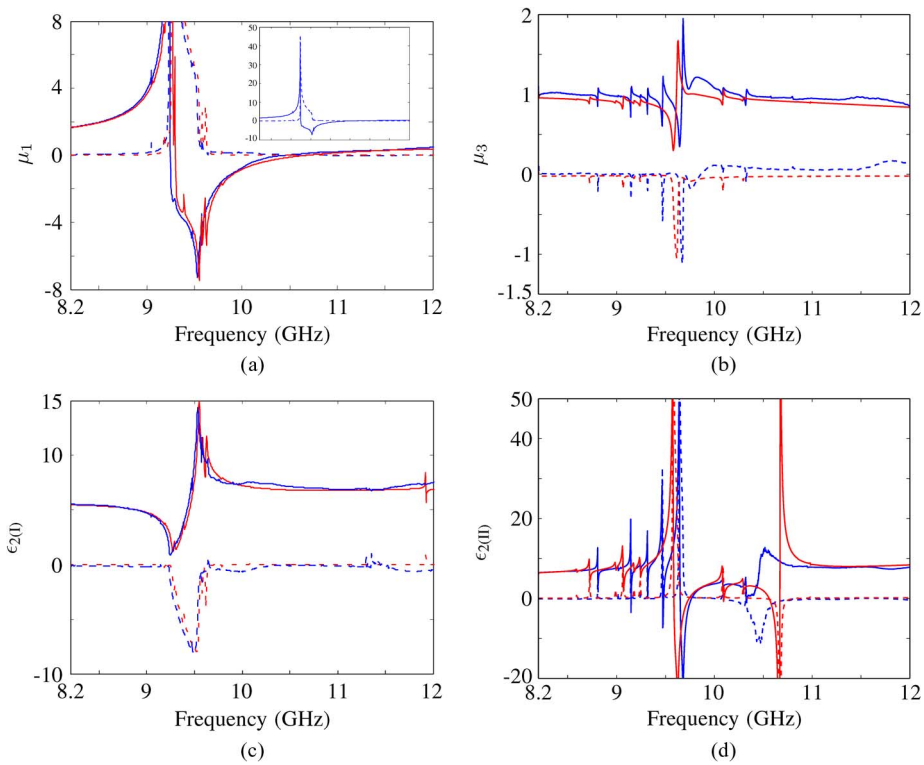

Fig. 5. Effective parameters extracted from waveguide measurements of the two oriented samples, with (a) zoomed in μ_1, (b) μ_3, (c) $\epsilon_{2(\mathrm{I})}$, and (d) $\epsilon_{2(\mathrm{II})}$. The blue and red curves are measurements and waveguide simulations, respectively. The solid and dashed curves represent the real ($'$) and imaginary ($''$) parts, respectively. The inset plot in (a) shows the measured μ_1 with the full vertical scale.

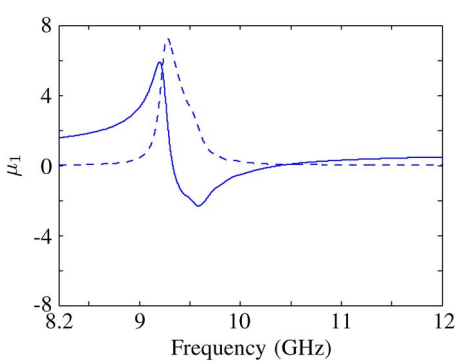

Fig. 6. Effective permeability μ_1 extracted from room temperature measurement of the copper SRR arrays on a Rogers 3010 substrate, plotted on the same scale as Fig. 5(a) for comparison. The solid and dashed blue curves represent the real ($'$) and imaginary ($''$) parts, respectively. The same measurement and calibration approach was used as in the cryogenic case.

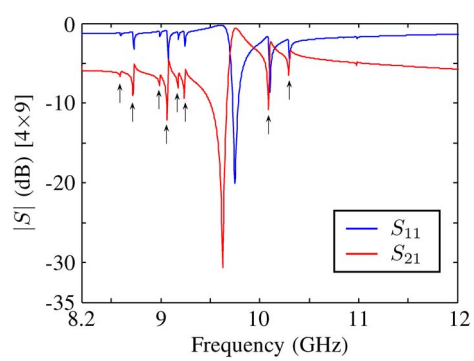

Fig. 7. Reflection (S_{11}, blue curve) and transmission (S_{21}, red curve) coefficients of the 4×9 SRR array sample from full-wave waveguide simulations. The markers indicate the locations of the sharp Fano-like resonances.

μ_1 and positive ϵ_2. Using the S parameters from these two measurements, the three parameters, i.e., μ_1, ϵ_2, and μ_3, are calculated from the formulas discussed earlier, with the results shown in Fig. 5. Near the resonances, (10) and (11) give two different effective permittivities along material axis 2. However, away from the resonant locations, the two have similar values.

The magnetic plasma frequency of this resonant structure is 10.45 GHz, $\mu_1' = 0$ in Fig. 5(a). Just below this frequency, between 9.25 and 10.45 GHz, the real part of the relative permeability μ_1' is negative, which is consistent with previously published work on SRRs. Generally, the imaginary part μ_1'', corresponding to loss, is large in this frequency band in room temperature normal conducting SRRs. The extracted value from the HTS SRR arrays, however, shows that at frequencies above the frequency where μ_1' is at its minimum, μ_1'' quickly drops to near zero. This is a property that is not observed in normal conducting SRRs on lossy substrates, as shown in the extracted μ_1 for the copper SRRs on a Rogers 3010 substrate (see Fig. 6). The Rogers 3010 substrate has a dielectric constant of 10.2 with a loss tangent of 0.0022 at 10 GHz [25]. The magnetic loss tangents ($\tan\,\delta_\mu = |\mu''/\mu'|$) for the Cu SRRs at $f(\mu'_{\min}) = 9.59$ GHz and $f(\mu'_{\min}) + 100$ MHz are 0.911 and 0.523, respectively, a 42% reduction. The $\tan\,\delta_\mu$ for the HTS SRRs at $f(\mu'_{\min}) = 9.53$ GHz and $f(\mu'_{\min}) + 100$ MHz are 0.324 and 0.068, respectively, a 79% reduction. In Fig. 5(c), we notice that ϵ'' is negative at frequencies just above where ϵ' is at a minimum. This is also seen in many published works on SRRs. A study of why different signs are seen for the imaginary

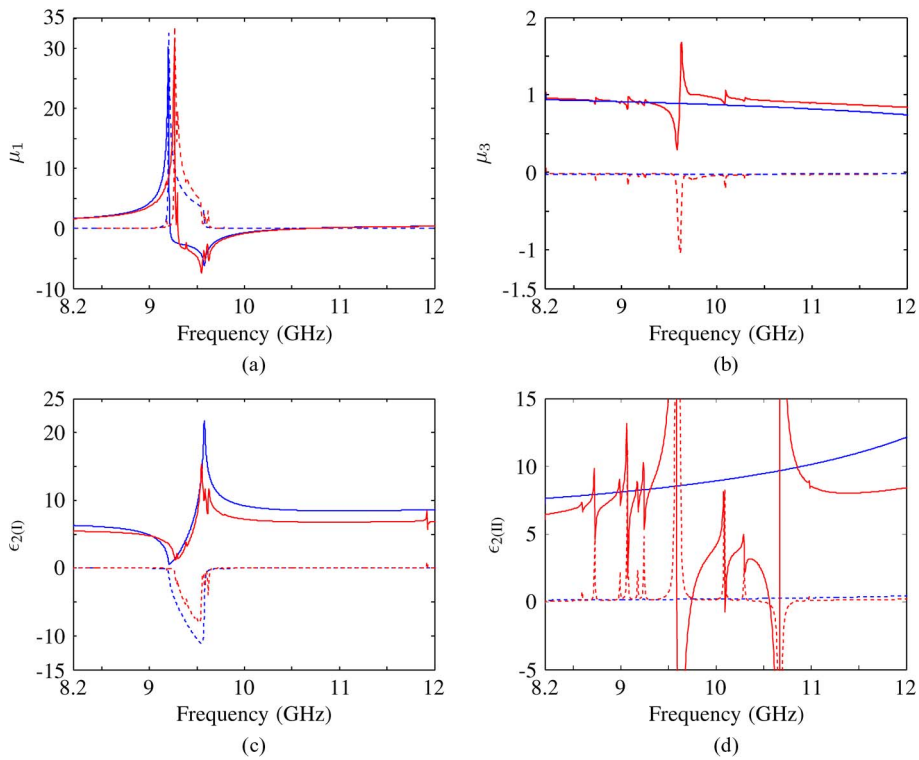

Fig. 8. Effective parameters extracted from the free-space and waveguide simulations of the two SRR arrays, with (a) μ_1 and (c) $\epsilon_{2(\mathrm{I})}$ from orientation I and (b) μ_3 and (d) $\epsilon_{2(\mathrm{II})}$ from orientation II. The red and blue curves represent the waveguide and free-space solutions, respectively. The solid and dashed curves are the real ($'$) and imaginary ($''$) parts, respectively.

parts of the constitutive parameters is beyond the scope of this paper. An explanation for this had been proposed by Koschny *et al.* [26]. In the frequency region where the effective permeability exhibits a resonant response, the effective permittivity exhibits an antiresonant response. This antiresonance is due to the finite lattice period of the metamaterial structure and gives rise to the negative ϵ'' shown in Fig. 5(c), as opposed to the positive μ'' shown in Fig. 5(a).

V. Comparison to Simulations

For comparison, the 4×1 SRR strips and 4×9 SRR samples placed inside the waveguide were modeled in the Ansys HFSS full-wave finite-element method simulator. In the simulations, a perfect electric conductor was used for the waveguide walls, the relative permittivity of MgO was set to 9.7 with a $\tan\delta$ of 5×10^{-6}, and the electrical conductivity of YBCO was set to 2.847×10^9 S/m, calculated from the sheet resistance of YBCO from [18]. The simulated S parameters from the orientation I and II models agree well with our low-temperature measurements. The multiple sharp resonances above and below the main resonances are also present, as shown in Fig. 7. The calculated effective parameters from the waveguide simulations are shown as solid and dashed red curves in Fig. 8. The effective μ_1 and $\epsilon_{2(\mathrm{I})}$ from the waveguide simulation are also plotted together with the measured results in Fig. 5(a) and (c), showing a 54-MHz offset. The effective μ_3 and $\epsilon_{2(\mathrm{II})}$ results are shown together in Fig. 5(b) and (d). Multiple sharp features are shown in both figures, corresponding to the sharp resonances shown in Figs. 4(b) and 7.

The free-space effective parameters of SRR arrays are of practical interest for applications such as metamaterial cloaks [10], [11]. Thus, free-space models of the SRR arrays were created in separate HFSS simulations and the effective parameters extracted for comparison and validation purposes. Electric and magnetic walls are assigned at the transverse boundaries to define the directions of the electric and magnetic fields ($\mathbf{E}$ parallel to axis 2) and to emulate a uniform plane wave normally incident on the SRR samples. For the free-space orientation I, the E- and H-fields are parallel to material axes 2 and 1, respectively. For the free-space orientation II, the E- and H-fields are parallel to material axes 2 and 3, respectively. In addition, the electric walls mirror the SRRs in the vertical direction to match the alternating arrangement of our HTS SRR arrays.

A set of scattering parameters is obtained for each of the orientations, from which the effective constitutive parameters are retrieved using the free-space extraction method discussed in [22] and [23]. The model with which the SRR array is aligned with orientation I allows for the extraction of μ_1 and $\epsilon_{2(\mathrm{I})}$, whereas orientation II allows for $\epsilon_{2(\mathrm{II})}$ and μ_3 extraction. These results are shown together with results from the waveguide simulations in Fig. 8 as blue solid and dashed curves. There is a slight offset in frequency between the two simulations: $f(\mu'_{1,\min})$ differ by 28 MHz, and $f(\epsilon'_{2\mathrm{I},\max})$ differ by 29 MHz. The offset is likely a result of imperfect meshing in the waveguide simulation, as further simulations suggest. The obvious disagreements from the two extraction techniques can be seen in the μ_3 and $\epsilon_{2(\mathrm{II})}$ curves. A reason for this is that the magnetic fields are present in both transverse and longitudinal directions inside the waveguide. They result in resonant behavior in both

orientations and give rise to the resonant feature seen in the waveguide μ_3 and $\epsilon_{2(\mathrm{II})}$, but not in the free-space μ_3 and $\epsilon_{2(\mathrm{II})}$. The antiresonant behavior at 10.66 GHz is a result from dividing by a near-zero μ_1 in (11).

VI. Discussion

In both the waveguide cryogenic measurement [see Fig. 4(b)] and the low-loss simulation (Fig. 7) of the 4×9 sample, the S parameters show eight high-Q resonances in addition to the main resonance, which are not seen in the low-loss free-space simulation. To the best of our knowledge, this is the first time such sharp and numerous features are observed in the waveguide measurement of SRR arrays. We are currently investigating their origin and will be reporting the findings in the near future. Kumley and Kuester [27] pointed out that high-Q resonances (referred to as Fano resonances) can arise from the slight variations in the structural dimension in the element array. However, the SRRs in the simulation have the same dimensions, thus ruling out this possibility. Similar sharp resonant features have also been observed by Kurter *et al.* [28]. These sharp dips in the electromagnetically induced transparency observed in this work are explained by the coupling of a gold (Au) strip and superconducting niobium (Nb) SRRs at sub-T_C, due to the large loss contrast between Au and Nb. In our experiments, only YBCO are used as the conducting material, and therefore, this loss differential does not exist. A single Fano or "trapped-mode" resonance has also been reported in [29] and [30] from free-space measurements of asymmetrical SRR arrays. The sharp resonances from our measurement have Q-factors $(f_r/\Delta f_{3\ \mathrm{dB}})$ as high as 1400, which is much higher than those observed in [29] for the asymmetrical SRR arrays also of YBCO thin films. In the case where the SRRs are made of copper on a Rogers 3010 substrate, room temperature measurements did not clearly reveal these high-Q features because the losses in the conductor and substrate damp them out. Details of the high-Q resonances will be reported in a separate article.

In summary, arrays of 4×1 strips and 4×9 YBCO SRR arrays were independently measured inside a WR-90 X-band waveguide at liquid nitrogen temperature. From the two sets of recorded S parameters, the effective constitutive parameters are retrieved where the SRR array is assumed to have an effective length and take on a homogeneous medium described by diagonal permittivity and permeability tensors. The extracted results from the measurements agree well with those from the low-loss waveguide and free-space full-wave simulations. The extracted effective permeability shows a negative μ' in the frequency band between 9.25 and 10.45 GHz, with the imaginary part μ'' quickly dropping to near zero close to the minimum of μ', a property not observed with room temperature normal conducting SRR arrays.

Acknowledgment

F. Trang would like to thank P. Dresselhaus for making the SRR contact mask and L. Vale for instruction and assistance on dicing the MgO wafer.

References

[1] U. Hasar and J. Barroso, "Permeability measurement of metamaterials with split-ring-resonators using free-space calibration-independent methods," *J. Infrared, Millim., Terahertz Waves*, vol. 33, no. 2, pp. 218–227, Feb. 2012.

[2] X. Chen, T. M. Grzegorczyk, B.-I. Wu, J. Pacheco, and J. A. Kong, "Robust method to retrieve the constitutive effective parameters of metamaterials," *Phys. Rev. E*, vol. 70, no. 1, Jul. 2004, Art. ID. 016608.

[3] D. R. Smith, S. Schultz, P. Markoš, and C. M. Soukoulis, "Determination of effective permittivity and permeability of metamaterials from reflection and transmission coefficients," *Phys. Rev. B*, vol. 65, no. 19, Apr. 2002, Art. ID. 195104.

[4] D. R. Smith, D. C. Vier, T. Koschny, and C. M. Soukoulis, "Electromagnetic parameter retrieval from inhomogeneous metamaterials," *Phys. Rev. E*, vol. 71, no. 3, Mar. 2005, Art. ID. 036617.

[5] Z. Szabo, G.-H. Park, R. Hedge, and E.-P. Li, "A unique extraction of metamaterial parameters based on Kramers–Kronig relationship," *IEEE Trans. Microw. Theory Techn.*, vol. 58, no. 10, pp. 2646–2653, Oct. 2010.

[6] X. Chen, T. M. Grzegorczyk, and J. A. Kong, "Optimization approach to the retrieval of the constitutive parameters of slab of general bianisotropic medium," *Prog. Electr. Res.*, vol. 60, pp. 1–18, 2006.

[7] H. Chen *et al.*, "Experimental retrieval of the effective parameters of metamaterials based on a waveguide method," *Opt. Exp.*, vol. 14, no. 26, pp. 12 944–12 949, Dec. 2006.

[8] R. A. Shelby, D. R. Smith, and S. Schultz, "Experimental verification of a negative index of refraction," *Science*, vol. 292, no. 5514, pp. 77–79, Apr. 2001.

[9] D. R. Smith *et al.*, "Design and measurement of anisotropic metamaterials that exhibit negative refraction," *IEICE Trans. Electron.*, vol. E87-C, no. 3, pp. 359–370, Mar. 2004.

[10] D. Schurig *et al.*, "Metamaterial electromagnetic cloak at microwave frequencies," *Science*, vol. 314, no. 5801, pp. 977–980, Oct. 2006.

[11] B. Kanté, D. Germain, and A. de Lustrac, "Experimental demonstration of a nonmagnetic metamaterial cloak at microwave frequencies," *Phys. Rev. B*, vol. 80, no. 20, Nov. 2009, Art. ID. 201104.

[12] F. Trang, H. Rogalla, and Z. Popović, "Resonant response of high-temperature superconducting split-ring resonators," *IEEE Trans. Appl. Supercond.*, vol. 23, no. 3, Jun. 2013, Art. ID. 1300405.

[13] N. Damaskos, R. Mack, A. Maffett, W. Parmon, and P. Uslenghi, "The inverse problem for biaxial materials," *IEEE Trans. Microw. Theory Techn.*, vol. 32, no. 4, pp. 400–405, Apr. 1984.

[14] M. Ricci, N. Orloff, and S. M. Anlage, "Superconducting metamaterials," *Appl. Phys. Lett.*, vol. 87, no. 3, Jul. 2005, Art. ID. 034102.

[15] M. C. Ricci and S. M. Anlage, "Single superconducting split-ring resonator electrodynamics," *Appl. Phys. Lett.*, vol. 88, no. 26, Jun. 2006, Art. ID. 264102.

[16] M. Ricci *et al.*, "Tunability of superconducting metamaterials," *IEEE Trans. Appl. Supercond.*, vol. 17, no. 2, pp. 918–921, Jun. 2007.

[17] H.-T. Chen *et al.*, "Tuning the resonance in high-temperature superconducting terahertz metamaterials," *Phys. Rev. Lett.*, vol. 105, no. 24, Dec. 2010, Art. ID. 247402.

[18] Technical Datasheet Film Coating. [Online]. Available: http://www.theva.com

[19] J. Mazierska, D. Ledenyov, M. V. Jacob, and J. Krupka, "Precise microwave characterization of MgO substrates for HTS circuits with superconducting post dielectric resonator," *Supercond. Sci. Technol.*, vol. 18, no. 1, pp. 18–23, Jan. 2005.

[20] M. W. Hosking *et al.*, "The dielectric constant of liquid nitrogen over the frequency range 0.5 to 10.4 GHz," *Supercond. Sci. Technol.*, vol. 6, no. 7, pp. 549–552, Jul. 1993.

[21] D. R. Smith, J. Gollub, J. J. Mock, W. J. Padilla, and D. Schurig, "Calculation and measurement of bianisotropy in a split ring resonator metamaterial," *J. Appl. Phys.*, vol. 100, no. 2, Jul. 2006, Art. ID. 024507.

[22] A. M. Nicolson and G. F. Ross, "Measurement of the intrinsic properties of materials by time-domain techniques," *IEEE Trans. Instrum. Meas.*, vol. IM-19, no. 4, pp. 377–382, Nov. 1970.

[23] W. Weir, "Automatic measurement of complex dielectric constant and permeability at microwave frequencies," *Proc. IEEE*, vol. 62, no. 1, pp. 33–36, Jan. 1974.

[24] Rohacell Dielectric Properties. [Online]. Available: http://www.rohacell.com

[25] Ro3000 Series Circuit Materials. [Online]. Available: http://www.rogerscorp.com

[26] T. Koschny, P. Markoš, D. R. Smith, and C. M. Soukoulis, "Resonant and antiresonant frequency dependence of the effective parameters of metamaterials," *Phys. Rev. E*, vol. 68, no. 6, Dec. 2003, Art. ID. 065602.

[27] K. Kumley and E. F. Kuester, "Effect of scatterer size variations on the reflection and transmission properties of a metafilm," in *Proc. USNC-URSI*, 2012.
[28] C. Kurter *et al.*, "Classical analogue of electromagnetically induced transparency with a metal–superconductor hybrid metamaterial," *Phys. Rev. Lett.*, vol. 107, no. 4, Jul. 2011, Art. ID. 043901.
[29] V. Fedotov *et al.*, "Temperature control of fano resonances and transmission in superconducting metamaterials," *Opt. Exp.*, vol. 18, no. 9, pp. 9015–9019, Apr. 2010.
[30] V. A. Fedotov, M. Rose, S. L. Prosvirnin, N. Papasimakis, and N. I. Zheludev, "Sharp trapped-mode resonances in planar metamaterials with a broken structural symmetry," *Phys. Rev. Lett.*, vol. 99, no. 14, Oct. 2007, Art. ID. 147401.

Frank Trang, biography not available at the time of publication.

Horst Rogalla (M'96–SM'14) was born in 1947. He received the Ph.D. degree in physics from Westfälische Wilhelms-Universität Münster, Münster, Germany, in 1979.

In 1977, he joined the Faculty of Physics, University of Giessen, Giessen, Germany, where he habilitated in 1986. Since 1987, he has been a Professor with the Department of Applied Physics, University of Twente, Enschede, The Netherlands, and is the Head of the Low Temperature Division. He is with the National Institute of Standards and Technology, Boulder, CO, USA, and also with the Department of Electrical Engineering, University of Colorado, Boulder. He is active in the university institutes, i.e., MESA+ Institute for Nanotechnology, Institute for Energy and Resources (IMPACT), and the Institute for Biomedical Technology and Technical Medicine. His research interests are in superconducting electronics and materials science, particularly related to thin-film growth and properties.

Dr. Rogalla is a member of the Dutch, German, and American Physical Societies, as well as the American and European Materials Research Society. He heads the European Superconducting Electronics network, i.e., Fluxonics, and is a Board Member of the European Society for Applied Superconductivity, after being its President for many years.

Zoya Popović (S'86–M'90–M'99–F'02) received the Dipl.Ing. degree from the University of Belgrade, Belgrade, Serbia, Yugoslavia, in 1985, and the Ph.D. degree from the California Institute of Technology, Pasadena, CA, USA, in 1990.

Since 1990, she has been with the University of Colorado, Boulder, CO, USA, where she is currently a Distinguished Professor and holds the Hudson Moore Jr. Chair with the Department of Electrical, Computer, and Energy Engineering. In 2001, she was a Visiting Professor with the Technical University of Munich, Munich, Germany. Since 1991, she has graduated 44 Ph.D. students. Her research interests include high-efficiency, low-noise, and broadband microwave and millimeter-wave circuits, quasi-optical millimeter-wave techniques, active antenna arrays, and wireless powering for batteryless sensors.

Prof. Popović was the recipient of the 1993 and 2006 Microwave Prizes presented by the IEEE Microwave Theory and Techniques Society for the Best Journal Papers and the 1996 URSI Issac Koga Gold Medal. In 1997, Eta Kappa Nu students chose her as a Professor of the Year. She was the recipient of a 2000 Humboldt Research Award for Senior U.S. Scientists of the German Alexander von Humboldt Stiftung. She was elected a Foreign Member of the Serbian Academy of Sciences and Arts in 2006. She was also the recipient of the 2001 Hewlett-Packard/American Society for Engineering Education Terman Medal for combined teaching and research excellence.